Relaxation Dynamics in the Merging of N Independent Condensates

M. Aidelsburger, J. L. Ville, R. Saint-Jalm, S. Nascimbène, J. Dalibard, and J. Beugnon
Laboratoire Kastler Brossel, Collège de France, CNRS, ENS-PSL Research University, UPMC-Sorbonne Universités, 11 place Marcelin-Berthelot, 75005 Paris, France
(Received 7 May 2017; revised manuscript received 26 September 2017; published 6 November 2017)

Controlled quantum systems such as ultracold atoms can provide powerful platforms to study nonequilibrium dynamics of closed many-body quantum systems, especially since a complete theoretical description is generally challenging. In this Letter, we present a detailed study of the rich out-of-equilibrium dynamics of an adjustable number N of uncorrelated condensates after connecting them in a ring-shaped optical trap. We observe the formation of long-lived supercurrents and confirm the scaling of their winding number with N in agreement with the geodesic rule. Moreover, we provide insight into the microscopic mechanism that underlies the smoothening of the phase profile.

DOI: 10.1103/PhysRevLett.119.190403

Thermalization of closed out-of-equilibrium many-body systems lies at the heart of statistical physics. Because of the recent progress in the preparation of well-controlled isolated quantum systems, this question can now be revisited in a quantum context [1]. Whereas most systems are expected to reach thermal equilibrium, nontrivial situations can occur in integrable systems [2], in the presence of disorder [3] or due to the formation of long-lived topological defects [4,5]. Out-of-equilibrium dynamics are also central to the study of dynamical crossings of phase transitions. Indeed, the divergence of the relaxation time at the critical point for a second-order phase transition entails that the system cannot follow adiabatically the external perturbation. The relaxation dynamics can be used in that case to determine the critical exponents of the phase transition [5].

A rich situation occurs when N condensates, characterized by independent initial phase factors, are coupled together. Let us consider, for instance, the case where the condensates are placed along a ring and connections are suddenly established between neighboring condensates. One expects that, after some transient dynamics, stochastic metastable supercurrents are formed. This ring geometry was put forward by Zurek in a seminal paper [6] drawing a parallel between laboratory experiments with liquid helium and classes of early universe theories. More recently this gedankenexperiment inspired experiments with superconducting loops [7–9] and cold atoms [10]. A key ingredient of Zurek's study is the relation between the winding number of the supercurrent and the number of initial condensates N according to the *geodesic rule*. In essence, it enables a computation of the winding number based on the minimization of the kinetic energy of the system.

In this Letter we investigate the relaxation dynamics of up to $N = 12$ uncorrelated Bose-Einstein condensates (BECs) after merging them in a ring-shaped optical trap. We measure the statistical distribution of metastable supercurrents and relate their emergence to the evolution of the

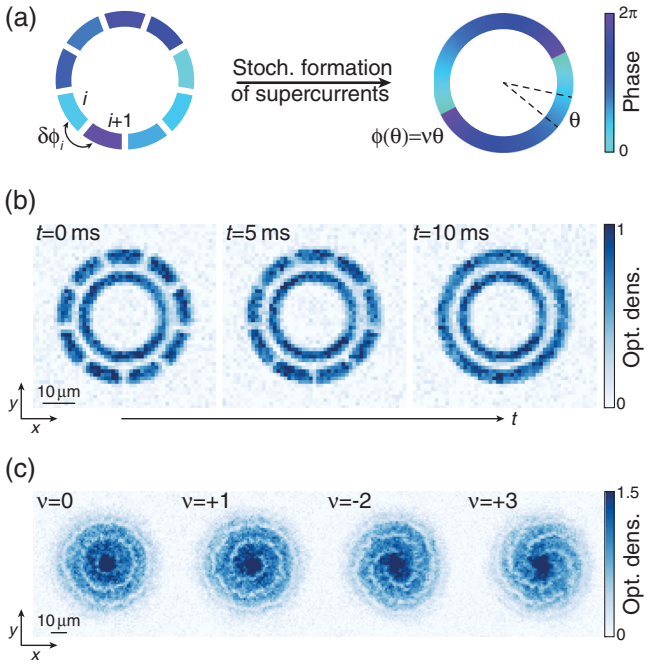

FIG. 1. Experimental protocol. (a) Illustration of the experimental sequence. An annular trap is partitioned into N segments of equal length. Uncorrelated BECs are prepared in these segments with random phase differences $\delta\phi_i$, $i = 1, \ldots, N$, between adjacent condensates. After merging into a single annular condensate, supercurrents with winding number $\nu \in \mathbb{Z}$ are formed. (b) *In situ* density distribution in the ring trap for $N = 9$ at different times t during the merging. The outer ring has a mean radius of 19.5 μm and a width of 5 μm. The inner ring serves as a phase reference for the detection as described in the main text. It has a mean radius of 13 μm and a width of 4 μm. Each image is an average over 5 or 6 experimental realizations. (c) Matter-wave interference after a 2D time of flight (TOF) of 6 ms. The chirality of the pattern and the number of spiral arms reveal the winding number ν of the supercurrent in the outer ring.

phase defects generated at the boundaries of the BECs. The experimental protocol is depicted in Fig. 1(a). Initially the condensates are characterized by random phase differences $\delta\phi_i$ $(i = 1, \ldots, N)$ between condensates i and $i+1$, that can lead to a net phase accumulation around the ring after merging [Fig. 1(b)]. Because of the single-valuedness of the wave function, the phase winding around the ring has to be equal to $2\pi\nu$, with winding number $\nu \in \mathbb{Z}$. This corresponds to the formation of supercurrents with quantized velocities, which we detect through matter-wave interference [Fig. 1(c)] with an additional ring-shaped condensate with uniform phase [10,11]. Our results show that the magnitude of the supercurrent scales in quantitative agreement with the geodesic rule. This extends earlier works on the merging of two [12] and three [13] condensates in a harmonic trap and on the dynamics of a large number of condensates in a two-dimensional (2D) optical lattice [14]. Complementary results have been obtained with a large number of Josephson junctions, where the scaling with N appears to be modified compared to the one studied in our work [7]. Additionally we explore the underlying dynamics by merging pairs of neighboring condensates. First, we study it globally by monitoring the evolution of the winding-number distribution as a function of time. Second, we detect local phase defects and study their dynamics in a time-resolved manner. The observed relaxation time scales are compatible with the evolution of solitonlike phase defects.

The experiment started by loading a cold cloud of $1.4(2) \times 10^5$ ^{87}Rb atoms in the $|F = 1, m_F = 0\rangle$ state into a pancake-type dipole trap with tight harmonic confinement along the vertical direction, $\omega_z = 2\pi \times 1.58(1)$ kHz, and negligible confinement in the xy-plane [15,16]. The in-plane trap was shaped using a digital micromirror device (DMD) in direct imaging with an optical resolution of ~ 1 μm to create a uniform double-ring trap as illustrated in Fig. 1(b). All experimental studies were performed in the outer ring, which was partitioned into several segments, while the inner ring served as a uniform phase reference for detection [10,11]. The distance between the segments as well as between the two rings was $2.5(2)$ μm, defined as the full width at half maximum of the density dip in the measured *in situ* distributions [Fig. 1(b)]. This separation is large enough to enable the formation of uncorrelated condensates [16].

After 2 s evaporative cooling, we reached a final temperature of $T < 20$ nK, thereby entering the quasi-2D regime $k_B T < \hbar\omega_z$, with k_B the Boltzmann constant and $\hbar$ the reduced Planck constant. The upper temperature limit of 20 nK is the smallest detectable temperature using our calibration method. This corresponds to 2D phase-space densities $\mathcal{D} = \lambda_T^2 n > 80$ deeply in the superfluid regime [18]; here $n = 36(4)/\mu\text{m}^2$ is the 2D atomic density, $\lambda_T = \hbar\sqrt{2\pi/(m k_B T)}$ the thermal wavelength and m the mass of one atom.

Subsequently, we merged the BECs in the outer ring within 10 ms by decreasing the width of the potential barriers [Fig. 1(b)] using our dynamically configurable DMD. The velocity at which the barriers were closed was chosen small compared to the speed of sound c_0 in order to prevent the formation of shock waves and high-energy excitations [19,20]. For our experimental parameters $c_0 = \sqrt{n g_{2D}/m} \approx 1.4(1)$ mm/s, where $g_{2D} = g_{3D}/(\sqrt{2\pi} l_z)$ is the 2D interaction parameter, $g_{3D} = 4\pi\hbar^2 a/m$, $a = 5.3$ nm the scattering length, and $l_z = \sqrt{\hbar/(m\omega_z)} = 0.27$ μm the harmonic oscillator length.

After a typical relaxation time of 0.5 s, we detected the phase winding after 2D time of flight by releasing the in-plane confinement abruptly while keeping the vertical one. We recorded the resulting interference pattern after 6 ms using standard absorption imaging along the z direction [Fig. 1(c)]. The chirality of the pattern and the number of spiral arms are a direct measure of the winding number ν of the supercurrent that was formed in the outer ring [10,11]. In an independent calibration measurement we found that

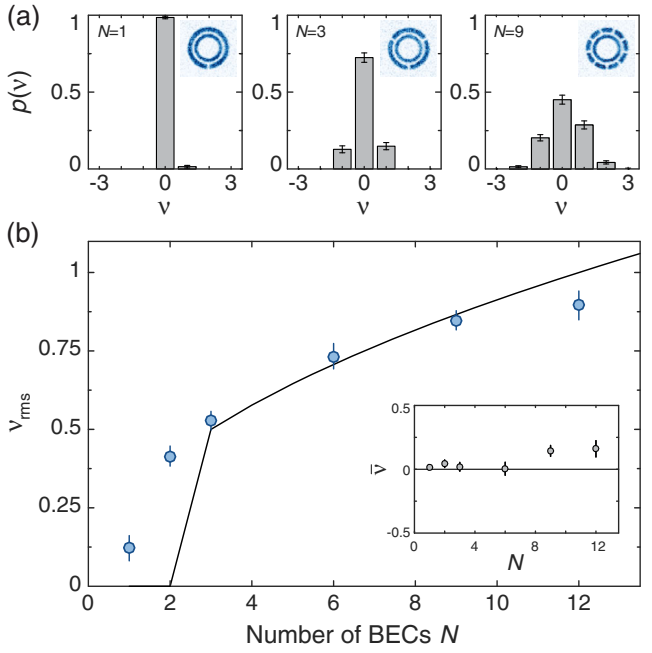

FIG. 2. Formation of supercurrents as a function of the number of BECs N. (a) Probability distributions $p(\nu)$ for $N = 1$, 3 and 9 obtained from $\mathcal{M} = 202$, 238, and 388 measurements, respectively. The insets display *in situ* images before the merging averaged over 4–6 realizations. (b) Measured rms width ν_{rms} of the probability distributions as a function of N. Each data point consists of $\mathcal{M} > 200$ independent measurements. The corresponding mean values $\bar{\nu}$ are displayed in the inset. The solid line is the predicted scaling given in Eq. (1). All error bars display the combined uncertainty from the experimental determination of the winding number and the statistical error due to a finite number of measurements $\mathcal{M}$, which was evaluated using a bootstrapping approach.

the probability of creating a supercurrent in the inner ring was $\lesssim 0.6\%$ [16].

Each repetition of the experiment results in a different set of random phase differences $\delta\phi_i$ that leads to the formation of a supercurrent with winding number $\nu = \sum_{i=1}^{N} \delta\phi_i/(2\pi)$, where $-\pi < \delta\phi_i \leq \pi$. The interval for the phase differences $\delta\phi_i$ is chosen according to the geodesic rule, which expresses the fact that the system tends to minimize the absolute value of the relative phase between neighboring condensates due to energetic reasons [21,22]. By repeating the measurement $\mathcal{M}$ times we extracted the corresponding probability distributions $p(\nu)$ as illustrated in Fig. 2(a). We observe an increase of the probability for nonzero winding numbers with N resulting in a broadening of the distribution. The measured center $\bar{\nu} = \sum_\nu p(\nu)\nu$ and rms width $\nu_{\mathrm{rms}} = \sqrt{\mathcal{M}/(\mathcal{M}-1)\sum_\nu p(\nu)(\nu-\bar{\nu})^2}$ of the individual distributions are depicted in Fig. 2(b).

Ideally the smallest number of domains that allows for the formation of topological defects is three. In this case the probabilities $p_{\mathrm{th}}(\nu)$ can be computed following simple arguments [13,23]. There are three possible cases: if $\delta\phi_1 + \delta\phi_2 > \pi$, the total sum of all phase differences has to amount to 2π, if $\delta\phi_1 + \delta\phi_2 < -\pi$ the total sum amounts to -2π and for all other cases it vanishes. The resulting probabilities are $p_{\mathrm{th}}(+1) = p_{\mathrm{th}}(-1) = 1/8$, which is compatible with our experimental results $p(+1) = 0.15(2)$ and $p(-1) = 0.13(2)$ displayed in Fig. 2(a). In general the probability distribution is determined by the Euler-Frobenius distribution [24] and we obtain

$$\nu_{\mathrm{rms}}(N) = \begin{cases} 0, & \text{if } N < 3 \\ \frac{1}{2\sqrt{3}}\sqrt{N}, & \text{if } N \geq 3. \end{cases} \quad (1)$$

The distribution is symmetric around $\nu = 0$, with $\bar{\nu} = 0$, which is in agreement with our experimental data obtained for small N [Fig. 2(b)]. For $N \geq 9$ there seems to be a small systematic shift to positive values.

Our experimental results shown in Fig. 2(b) are in agreement with the predicted scaling for $N \geq 3$. There is a discrepancy for $N = 1$, where we measure a nonzero probability for the formation of supercurrents $p(\nu \neq 0) = 1.5(8)\%$. We attribute this to phase fluctuations of the condensate due to finite temperature effects, which are enhanced for larger systems. We tested that reducing the radius of the condensate by one-third significantly reduces the probability for nonzero winding numbers. For $N \geq 3$ thermal fluctuations are not expected to have a large influence because the length of the condensates is smaller. Regarding the case of $N = 2$ we found that this particular configuration was very sensitive to the alignment of our trap. Small trap inhomogeneities had a significant impact on the obtained distributions.

For the largest number of condensates $N = 12$ we measure slightly smaller values than expected, most likely due to an increased sensitivity to experimental imperfections and overlapping time scales. If the merging of the BECs is performed too slowly, there are two main effects that can lead to a reduction of ν_{rms}. If supercurrents are already formed during the merging, their lifetime could be reduced substantially due to the presence of residual weak potential barriers [25]. At the same time an asynchronous merging of the barriers could effectively reduce the total number of initial condensates, if the phase of neighboring condensates homogenizes before the merging is complete. We have investigated this in more detail for $N = 9$ and found a significant reduction of the winding numbers for merging times larger than 50 ms [16]. Both effects are expected to be more critical for increasing N.

We typically wait 0.5 s after merging the condensates before detecting the supercurrents. This waiting time is short compared to the lifetime of the supercurrents in our trap [16]. Indeed we observe no significant decay of the supercurrents for waiting times on the order of 10 s. On the other hand it is long enough to let the system relax to a steady state with a smoothened phase profile, without a significant number of defects in the interference pattern.

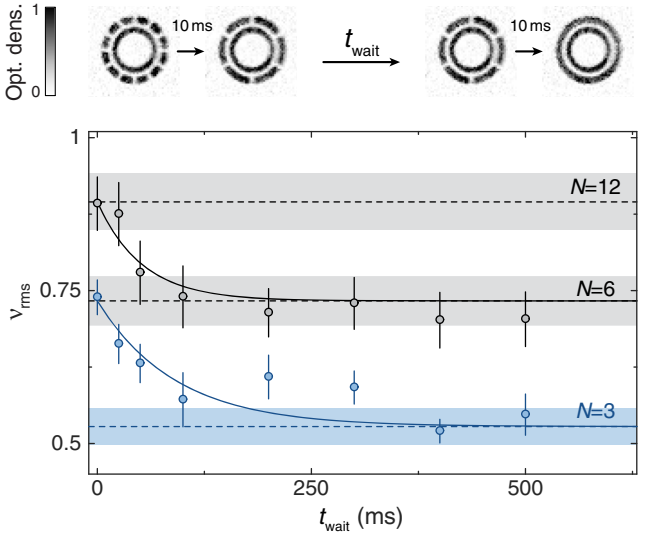

FIG. 3. Relaxation dynamics from N to $N/2$ condensates, when merging them in two successive steps. The *in situ* images above the main graph illustrate the experimental sequence for $N = 12$. Each image is an average over five individual measurements. The main graph depicts our experimental results for $N = 12$ (black) and $N = 6$ (blue). Each data point consists of $\mathcal{M} > 200$ measurements. The corresponding mean values $\bar{\nu}$ are shown in the Supplemental Material [16]. The error bars depict the uncertainty obtained from our finite number of measurements $\mathcal{M}$ and the experimental uncertainty in the determination of the winding numbers. The dashed lines indicate the measured values shown in Fig. 2(b) and the shaded areas illustrate the corresponding error bars. The solid lines are fits of exponential functions $f_j(t_{\mathrm{wait}}) = A_j e^{-t_{\mathrm{wait}}/\tau_j} + B_j$, $j = \{6, 12\}$, to our data, where τ_j is the only free fit parameter and the other variables are determined by the dashed lines extracted from Fig. 2(b).

In order to gain a deeper insight into the underlying relaxation dynamics, we performed two separate experiments. First, we probed the evolution of the winding number distribution by merging the BECs on the ring in two successive steps. The sequence started by merging pairs of neighboring condensates within 10 ms to reduce the number of condensates by a factor of 2, then we let the system relax for a variable time t_{wait} and subsequently merged the remaining $N/2$ condensates in 10 ms into a single annular BEC (Fig. 3). After an additional evolution time of 0.5 s we detected the probability distributions $p(\nu)$ using the detection method explained above.

We identify two limiting cases for the data shown in Fig. 3. If there is no additional wait time ($t_{\mathrm{wait}} = 0$) between the two merging steps, the system has not enough time to relax and the probability distribution resembles the one discussed in Fig. 2, where all condensates were merged in a single step. On the other hand, if t_{wait} is longer than the relaxation time, the phase of neighboring condensates homogenizes after the first step, so that we effectively reduce the number of initial phase domains to $N/2$ and the distribution approaches the one for $N/2$ initial BECs merged in a single step. The measurements were performed for $N = 12$ and $N = 6$ and the dashed lines indicate the limiting cases explained above. In order to extract a time scale for the relaxation, we fit an exponential decay to each of the two data sets. The amplitude and offset of the fitting function are determined by the data points displayed in Fig. 2(b). One can infer two different time scales $\tau_{12} = 52(17)$ ms and $\tau_6 = 90(30)$ ms associated with the relaxation dynamics, which most likely depend on the spatial extent of the condensates, that differ by almost a factor of 2 for the two data sets.

In a second set of measurements we focus on the microscopic relaxation dynamics via the time-resolved detection of local phase defects. We merged two condensates and probed the evolution of the phase profile through interference with a reference condensate [Fig. 4(a)]. The length of each condensate is comparable to the length of one segment studied in the relaxation dynamics discussed above for $N = 6$. At short times (~1 ms), we observe a phase defect in the center of the fringes, at the original position of the potential barrier [Fig. 4(b)]. With increasing time more phase defects appear and also start to propagate. After 5 ms the number of defects decays and we find an almost uniform distribution of their positions [26]. At long times (>100 ms) almost all defects have disappeared in agreement with the results displayed in Fig. 3.

We interpret the observed dynamics by the formation of dark solitons at the position of the potential barrier, whereby their shape depends on the random phase differences between neighboring condensates [27–29]. Subsequently, the generated excitations propagate, interact with each other, and eventually decay [29,30] to form a steady state with a smoothened phase profile [Figs. 3(b) and 3(c)]. Note, that the lifetime of solitonic excitations is typically short for 3D systems but can be strongly enhanced in low-dimensional geometries [31–33]. The propagation speed of dark solitons depends on their depth and is at maximum equal to the speed of sound c_0, which is compatible with the observed relaxation time scales. The round-trip time at c_0 in the ring trap is about 90 ms for the configuration studied in Fig. 2.

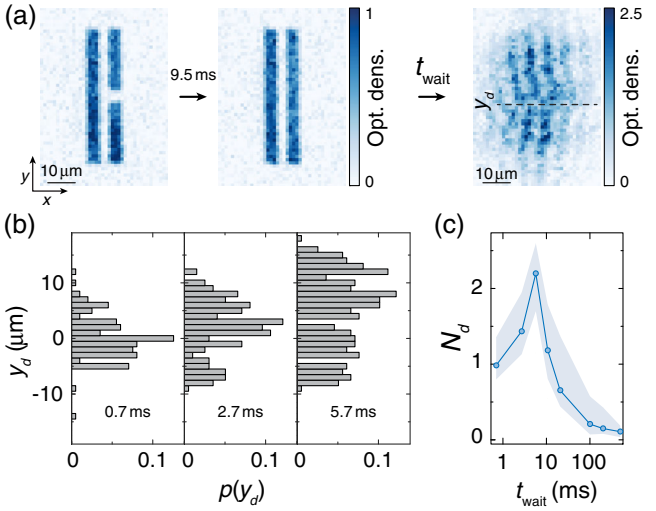

FIG. 4. Defect dynamics. (a) *In situ* density distribution of two line-shaped condensates (first two images) with dimensions 50 μm × 5 μm before and after the merging (averaged over four individual realizations). The condensates are separated by 3 μm. After merging the condensates in 9.5 ms the system evolves for a variable time t_{wait}. Phase defects are detected by matter-wave interference after TOF (image on the right) [16]. A typical image for $t_{\mathrm{wait}} = 0.7$ ms is depicted on the right. The phase defect at position y_d is highlighted by the dashed line. (b) Position distribution $p(y_d)$ of the phase defects as a function of the waiting time t_{wait} evaluated from 200 individual measurements. The histograms are normalized by the total number of measurements. Phase dislocations are detected, if the phase difference between neighboring pixels (corresponds to 1.16 μm in the atomic plane) is larger than 0.3π [16]. (c) Mean number of phase defects N_d as a function of time. The data were evaluated using a threshold of 0.3π. The shaded area illustrates the sensitivity due to this analysis (upper bound: 0.16π; lower bound: 0.43π).

In conclusion, we have reported the first quantitative study of the $\sqrt{N}$ scaling as predicted by the geodesic rule and show that the underlying relaxation dynamics is consistent with the formation of solitonlike defects. Future experiments could benefit from phase-imprinting techniques [27–29] to study the dynamics in a fully deterministic manner. In particular, it would be interesting to study the dynamics as a function of temperature and geometry.

We thank W. D. Phillips and S. Stringari for insightful discussions. This work was supported by DIM NanoK and

ERC (Synergy UQUAM). This project has received funding from the European Union's Horizon 2020 research and innovation program under the Marie Sklodowska-Curie Grant Agreement No. 703926.

[1] J. Eisert, M. Friesdorf, and C. Gogolin, Quantum many-body systems out of equilibrium, Nat. Phys. **11**, 124 (2015).
[2] T. Langen, T. Gasenzer, and J. Schmiedmayer, Prethermalization and universal dynamics in near-integrable quantum systems, J. Stat. Mech. (2016), P064009 (2016).
[3] R. Nandkishore and D. A. Huse, Many-body localization and thermalization in quantum statistical mechanics, Annu. Rev. Condens. Matter Phys. **6**, 15 (2015).
[4] T. Kibble, Phase-transition dynamics in the lab and the universe, Phys. Today **60**, 47 (2007).
[5] A. Del Campo and W. H. Zurek, Universality of phase transition dynamics: Topological defects from symmetry breaking, Int. J. Mod. Phys. B **29**, 1430018 (2014).
[6] W. H. Zurek, Cosmological experiments in superfluid helium?, Nature (London) **317**, 505 (1985).
[7] R. Carmi, E. Polturak, and G. Koren, Observation of Spontaneous Flux Generation in a Multi-Josephson-Junction Loop, Phys. Rev. Lett. **84**, 4966 (2000).
[8] R. Monaco, J. Mygind, and R. J. Rivers, Zurek-Kibble Domain Structures: The Dynamics of Spontaneous Vortex Formation in Annular Josephson Tunnel Junctions, Phys. Rev. Lett. **89**, 080603 (2002).
[9] R. Monaco, J. Mygind, R. J. Rivers, and V. P. Koshelets, Spontaneous fluxoid formation in superconducting loops, Phys. Rev. B **80**, 180501 (2009).
[10] L. Corman, L. Chomaz, T. Bienaimé, R. Desbuquois, C. Weitenberg, S. Nascimbène, J. Dalibard, and J. Beugnon, Quench-Induced Supercurrents in an Annular Bose Gas, Phys. Rev. Lett. **113**, 135302 (2014).
[11] S. Eckel, F. Jendrzejewski, A. Kumar, C. J. Lobb, and G. K. Campbell, Interferometric Measurement of the Current-Phase Relationship of a Superfluid Weak Link, Phys. Rev. X **4**, 031052 (2014).
[12] G. B. Jo, J. H. Choi, C. A. Christensen, T. A. Pasquini, Y. R. Lee, W. Ketterle, and D. E. Pritchard, Phase-Sensitive Recombination of Two Bose-Einstein Condensates on an Atom Chip, Phys. Rev. Lett. **98**, 180401 (2007).
[13] D. R. Scherer, C. N. Weiler, T. W. Neely, and B. P. Anderson, Vortex Formation by Merging of Multiple Trapped Bose-Einstein Condensates, Phys. Rev. Lett. **98**, 110402 (2007).
[14] V. Schweikhard, S. Tung, and E. A. Cornell, Vortex Proliferation in the Berezinskii-Kosterlitz-Thouless Regime on a Two-Dimensional Lattice of Bose-Einstein Condensates, Phys. Rev. Lett. **99**, 030401 (2007).
[15] J. L. Ville, T. Bienaimé, R. Saint-Jalm, L. Corman, M. Aidelsburger, L. Chomaz, K. Kleinlein, D. Perconte, S. Nascimbène, J. Dalibard *et al.*, Loading and compression of a single two-dimensional Bose gas in an optical accordion, Phys. Rev. A **95**, 013632 (2017).
[16] See Supplemental Material at http://link.aps.org/supplemental/10.1103/PhysRevLett.119.190403, which includes Ref. [17], for a detailed description of the experimental sequence, calibration measurements for the phase reference of the inner ring, measurements on the random phase difference between neighboring condensates, lifetime measurements of the supercurrents, mean values $\bar{\nu}$ of the distribution for the data depicted in Fig. 3, and details about the experimental sequence and data analysis for the results displayed in Fig. 4.
[17] R. T. Bailey, Estimation from Zero-Failure Data, Risk Analysis **17**, 375 (1997).
[18] According to the Mermin-Wagner theorem there is no true long-range order in low-dimensional systems; however, for our experimental parameters the characteristic correlation length exceeds the size of the condensate by several orders of magnitude, which enables the formation of a Bose-Einstein condensate.
[19] J. J. Chang, P. Engels, and M. A. Hoefer, Formation of Dispersive Shock Waves by Merging and Splitting Bose-Einstein Condensates, Phys. Rev. Lett. **101**, 170404 (2008).
[20] R. Meppelink, S. B. Koller, J. M. Vogels, P. van der Straten, E. D. van Ooijen, N. R. Heckenberg, H. Rubinsztein-Dunlop, S. A. Haine, and M. J. Davis, Observation of shock waves in a large Bose-Einstein condensate, Phys. Rev. A **80**, 043606 (2009).
[21] T. W. B. Kibble and A. Vilenkin, Phase equilibration in bubble collisions, Phys. Rev. D **52**, 679 (1995).
[22] S. Rudaz, A. M. Srivastava, and S. Varma, Probing gauge string formation in a superconducting phase transition, Int. J. Mod. Phys. B **14**, 1591 (1999).
[23] M. Bowick, L. Chandar, E. A. Schiff, and A. M. Srivastava, The cosmological kibble mechanism in the laboratory: string formation in liquid crystals, Science **263**, 943 (1994).
[24] S. Janson, Euler-Frobenius numbers and rounding, Online J. Anal. Comb. **8** (2013).
[25] A. Ramanathan, K. C. Wright, S. R. Muniz, M. Zelan, W. T. Hill III, C. J. Lobb, K. Helmerson, W. D. Phillips, and G. K. Campbell, Superflow in a Toroidal Bose-Einstein Condensate: An Atom Circuit with a Tunable Weak Link, Phys. Rev. Lett. **106**, 130401 (2011).
[26] The asymmetry in the position distribution of the phase defects [third panel of Fig. 4(b)] is due to a bias in the contrast of the interference fringes.
[27] S. Burger, K. Bongs, S. Dettmer, W. Ertmer, K. Sengstock, A. Sanpera, G. V. Shlyapnikov, and M. Lewenstein, Dark Solitons in Bose-Einstein Condensates, Phys. Rev. Lett. **83**, 5198 (1999).
[28] J. Denschlag, J. E. Simsarian, D. L. Feder, C. W. Clark, L. A. Collins, J. Cubizolles, L. Deng, E. W. Hagley, K. Helmerson, W. P. Reinhardt *et al.*, Generating solitons by phase engineering of a Bose-Einstein condensate, Science **287**, 97 (2000).
[29] C. Becker, S. Stellmer, P. Soltan-Panahi, S. Dörscher, M. Baumert, E.-M. Richter, J. Kronjäger, K. Bongs, and K. Sengstock, Oscillations and interactions of dark and dark–bright solitons in Bose–Einstein condensates, Nat. Phys. **4**, 496 (2008).
[30] E. A. Kuznetsov and S. K. Turitsyn, Instability and collapse of solitons in media with a defocusing nonlinearity, Sov. Phys. JETP **67**, 1583 (1988).

[31] C. Becker, K. Sengstock, P. Schmelcher, P. G. Kevrekidis, and R. Carretero-González, Inelastic collisions of solitary waves in anisotropic Bose–Einstein condensates: sling-shot events and expanding collision bubbles, New J. Phys. **15**, 113028 (2013).

[32] G. Lamporesi, S. Donadello, S. Serafini, F. Dalfovo, and G. Ferrari, Spontaneous creation of Kibble–Zurek solitons in a Bose–Einstein condensate, Nat. Phys. **9**, 656 (2013).

[33] S. Donadello, S. Serafini, T. Bienaimé, F. Dalfovo, G. Lamporesi, and G. Ferrari, Creation and counting of defects in a temperature-quenched Bose-Einstein condensate, Phys. Rev. A **94**, 023628 (2016).